Optical Strong Coupling between near-Infrared Metamaterials and Intersubband Transitions in III-Nitride Heterostructures

Alexander Benz,[†,‡] Salvatore Campione,[†,‡] Michael W. Moseley,[‡] Jonathan J. Wierer, Jr.,[‡] Andrew A. Allerman,[‡] Joel R. Wendt,[‡] and Igal Brener*[,†,‡]

[†]Center for Integrated Nanotechnologies (CINT), Sandia National Laboratories, P.O. Box 5800, Albuquerque, New Mexico 87185, United States

[‡]Sandia National Laboratories, P.O. Box 5800, Albuquerque, New Mexico 87185, United States

ABSTRACT: We present the design, realization, and character-ization of optical strong light−matter coupling between intersub-band transitions within a semiconductor heterostructures and planar metamaterials in the near-infrared spectral range. The strong light−matter coupling entity consists of a III-nitride intersubband superlattice heterostructure, providing a two-level system with a transition energy of ∼0.8 eV ($\lambda \sim 1.55\ \mu$m) and a planar "dogbone" metamaterial structure. As the bare metamaterial resonance frequency is varied across the intersubband resonance, a clear anticrossing behavior is observed in the frequency domain. This strongly coupled entity could enable the realization of electrically tunable optical filters, a new class of efficient nonlinear optical materials, or intersubband-based light-emitting diodes.

KEYWORDS: *metamaterials, nanocavities, strong light−matter interaction, intersubband transitions, near-infrared*
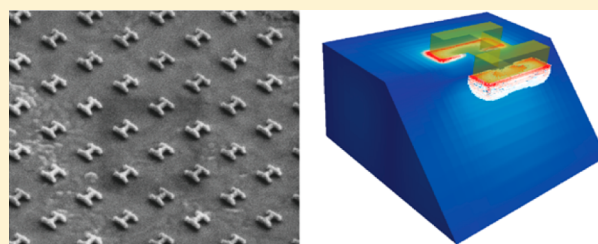
Optical strong light−matter coupling describes the phenomenon of energy oscillating between an optical cavity and a two-level system at a rate that is faster than all loss mechanisms present in the system. This periodic energy exchange can be observed as a beating in the time domain of various observables such as reflectance or transmittance[1] or in the frequency domain as a splitting of the single cavity resonance into two polariton branches.[2,3] The characteristic frequency for this exchange is called the vacuum Rabi frequency. Recently, strong light−matter coupling has been demonstrated experimentally in optical cavities with extremely small interaction volumes.[4−9] Particularly, metallic structures seem ideally suited due to their ability to confine the electromagnetic field to deep subwavelength volumes based on localized surface plasmons.[10,11] The low quality factor associated with metallic cavities (typical values are on the order of 10) can be overcome by coupling to two-level systems with large oscillator strengths. Previous results in the visible spectral range used subwavelength hole arrays, planar microcavities, or plasmonic dimers in combination with organic molecules (J-aggregates).[4,12,13] In the mid to long infrared wavelength region of the electromagnetic spectrum metamaterials combined with intersubband transitions (ISTs) in semiconductor heterostruc-tures are an attractive system,[6−9] due to the possibility to engineer all system parameters independently of each other. The properties of metamaterial resonators such as resonance frequency or cavity near field depend primarily on the geometry (size and shape). The transition energy of ISTs can be controlled by changing the dimensions of the potential wells formed by thin stacks of different energy gap semiconductors

grown on top of each other and can thereby be (mostly) decoupled from the underlying bulk crystals.

The strongly coupled entities formed by metamaterials and ISTs show great potential for the realization of nonlinear optical components,[14,15] electrically tunable optical filters,[16] or light-emitting diodes in the mid to long infrared wavelength range.[17] Higher order nonlinear processes ($\chi^{(2)}$, $\chi^{(3)}$, etc.) benefit from the giant nonlinearities that can be engineered using ISTs[18] and can be greatly amplified using metamaterials due to the strong electric field enhancement in their vicinity.[15] Electrical tuning of the spectral response in these systems can be achieved by altering the strength of the light−matter coupling. The transition energy of ISTs can be controlled by an external bias using the quantum-confined Stark effect.[19,20] This approach was used recently to demonstrate an electrically tunable optical filter at $\lambda \sim 10\ \mu$m with a tuning range of 8% of its center frequency.[16] By adapting the metamaterial and IST designs, the same approach can be used to realize optical filters and modulators in the entire spectral range from THz frequencies to potentially the visible. The strongly coupled metamaterial−IST entity can also be regarded as a planar array of individual polariton emitters[17] with subwavelength separa-tions, which could lead to an electrically pumped intersubband light-emitting diode (LED). The extremely fast energy exchange between metamaterial resonator and IST overcomes the fast, nonradiative scattering processes in ISTs,[21] which otherwise hinder efficient broadband light generation. All these potential devices require the unambiguous realization of strong
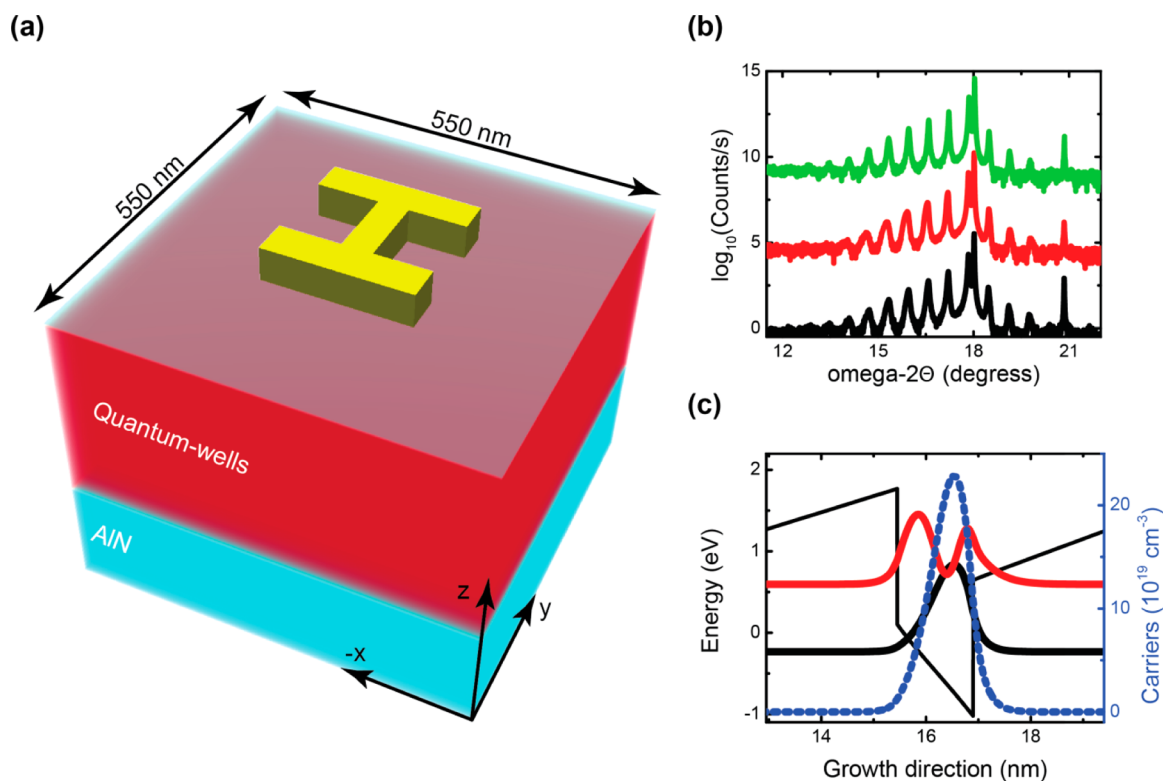
Figure 1. Unit-cell schematic and heterostructure properties (structural and optical). (a) The metamaterial nanocavity is fabricated on top of a quantum-well stack (red), grown on top of a 1.3 μm AlN buffer layer (blue). (b) X-ray diffraction omega−2θ scans about the (0002) reflection. The low (black line), medium (red line), and high (green line) doped samples show superlattice satellite peaks from $n = -9$ to $n = +7$, confirming the crystal quality of the heterostructure. The individual lines are offset vertically for clarity. (c) Calculated band structure for the medium doped sample $(1.6 \times 10^{20}$ cm$^{-3})$. The transition energy between ground (black) and first excited (red) state is 0.79 eV, corresponding to a transition wavelength of 1.56 μm. The free electrons are confined to the ground state, while the excited state is almost unpopulated.

light−matter coupling in the wavelength range of interest. However, pushing the strongly coupled metamaterial−IST system from the mid-infrared region to the near-infrared (NIR) and observing a clear signature for strong coupling has proven elusive in the past. The ratio of Rabi frequency to bare cavity frequency, which defines the visibility of the polariton splitting in a spectroscopic experiment, scales with the square root of the wavelength.[2] Previous implementations of strong coupling in the visible range using organic molecules[4,12] do not offer enough design flexibility in terms of transition energy or electrical tuning. More specifically, molecules with large oscillator strengths like J-aggregates emit only at visible wavelengths, and it is extremely difficult to design emitters with organic molecules in the near-IR.

Here we present the design, realization, and characterization of strong light−matter interaction between a planar metamaterial consisting of individual "dogbone" metamaterial nanocavities[8,22] and intersubband transitions in III-nitride heterostructures. The basic geometry of our system is presented in Figure 1a. The planar metamaterial is fabricated directly on top of an Al$_{0.03}$Ga$_{0.97}$N/AlN superlattice heterostructure. The III-nitride semiconductor provides an adequate conduction band offset to confine electronic states and provides a two-level system with a transition energy of ∼0.8 eV (∼1.55 μm). The planar metamaterial acts as the optical cavity and couples the free space radiation to the ISTs. We analyze the light−matter coupling theoretically and experimentally for three different doping levels larger than 8×10^{19} cm^{-3} by studying the optical transmittance at normal incidence. We demonstrate an

experimental Rabi frequency of 10.1 THz corresponding to a polariton splitting of 10% of the center frequency. Furthermore, we calculate an interaction volume of 1.21×10^{-3} $(\lambda/n)^3$ for an individual metamaterial nanocavity.

The Al$_{0.03}$Ga$_{0.97}$N/AlN superlattice heterostructures are grown on (0001) c-plane sapphire substrates using metal−organic vapor phase epitaxy. A ∼1.3 μm thick AlN buffer is grown prior to the heterostructure to reduce the effects of the lattice mismatch to the substrate and thereby mitigate the strain. The heterostructure consists of 40 pairs of 1.45 nm thick quantum wells (QWs) and 4.5 nm thick AlN barriers, resulting in a transition energy of 0.79 eV or a transition wavelength of 1.56 μm. The growth is capped with a 4 nm thick AlN barrier; the choice of the thin cap layer will be explained later. Three different samples are grown with different homogeneously silicon-doped QWs: 8×10^{19} cm^{-3} (here referred to as the low doping level), 1.6×10^{20} cm^{-3} (medium doping), and 2.4×10^{20} cm^{-3} (high doping). We would like to point out here that the realization of high-quality AlGaN-based heterostructures is very demanding. An inherent lattice mismatch of 2.5% exists between AlN and GaN that adds strain to the crystal and limits the maximum thickness of the heterostructure.[23] The choice of AlN templates over GaN templates avoids tensile strain induced cracking and enables pseudomorphic growth of superlattice heterostructures up to approximately 1 μm thickness with the average aluminum composition of 0.76 used in this work.[24] The total thickness for the 40-period superlattice heterostructure in this work is 238 nm, thus significantly less than the approximate pseudomorphic limit for
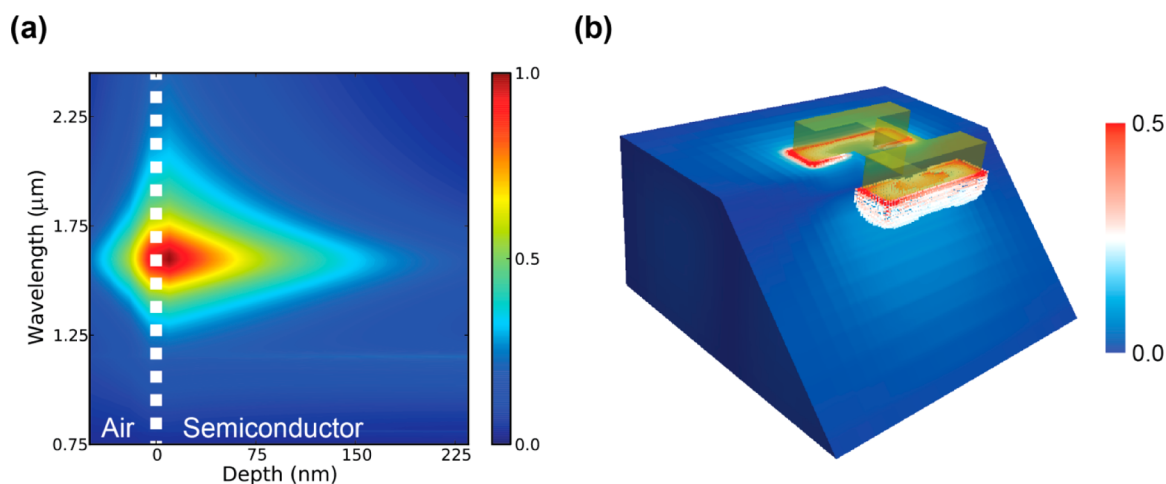
(a)

(b)

Figure 2. Calculated electric field profiles polarized along the z-axis. (a) The bare metamaterial nanocavity has its fundamental resonance at 1.56 μm. The peak value for the E_z field is located close to the metal (at the air–semiconductor interface) inside the semiconductor. A strong E_z field extends approximately 150 nm into the semiconductor. Since the influence of the intersubband transition is removed in this simulation, all three samples give the same near field profile. (b) Cut through the unit-cell showing the E_z field on resonance (1.56 μm). The field remains concentrated underneath the metal traces. The symbols indicate the regions with the strongest E_z field.

growth on AlN. Even if the strain can be handled correctly, the high growth temperatures (~1050 °C) in metal organic vapor phase epitaxy reactors cause GaN/AlGaN superlattice hetero-structures doped with Si at concentrations exceeding 10^{19} cm^{-3} to undergo significant layer intermixing.[25] To avoid this problem, we worked at significantly lower growth temperature (~800 °C), which efficiently suppressed layer intermixing, resulting in sharper interfaces.[25,26] To verify the crystal quality of our superlattice heterostructure, X-ray diffraction omega−2θ scans about the (0002) reflection were taken. The scans for the low, medium, and high doped samples are presented in Figure 1b, showing superlattice satellite peaks from $n = -9$ to $n = +7$. The energy states of the QWs are calculated using a self-consistent band structure simulation based on the eight-band k·p method. The simulation includes the effects of free carriers, the electrostatic potential due to the ionized donor atoms, and the piezoelectric and spontaneous polarization-induced electric fields present in wurtzite AlGaN c-plane heterostructures. The simulation result for the medium doping level sample is shown in Figure 1c. The Fermi level is located between the ground state and the first excited state within the QW, so that almost all the free carriers are confined to the ground state. The predicted transition energy is confirmed by measuring the intersubband absorption in a multipass waveguide geometry. The peak absorption is centered at ~1.52 μm regardless of doping concentration, which is in good agreement with the band structure simulations.

To simulate the strongly coupled system, we use a commercial finite-difference time-domain (FDTD) simulation package.[27] We model one unit cell (shown in Figure 1a) with periodic boundary conditions that mimic the effect of the two-dimensional metamaterial array in the real device. The material parameters for the gold resonators are extracted from spectral ellipsometry measurements[28] on a separate 100 nm thin gold film prepared under identical conditions as the samples. The ISTs are modeled as anisotropic harmonic oscillators following the dipole selection rules for ISTs in GaN heterostructures. Only light polarized along the growth direction of the crystal (here labeled z-axis) can excite the IST.[29] Therefore, we have to provide a means to convert energy from the normal incidence

radiation that propagates along the z-axis and contains therefore no z-polarized electric field in the far field. Planar metamaterial resonators are one possible solution to provide the correct polarization in their near field, which allows for coupling free-space radiation to ISTs.[30] We present the spectrally and spatially resolved near field for the bare cavity (no quantum-well interaction), showing the electric field polarized along the z-axis in Figure 2a. The simulations show one clear resonance and a non-negligible E_z component that extends approximately 150 nm into the semiconductor. The largest amplitude of the E_z field is very close to the air–semiconductor interface, and this is the reason for the choice of a 4 nm cap layer atop the heterostructure. At the same time, the rapidly decaying E_z field also defines the maximum useful thickness of the heterostructure. Since the ISTs can interact with only the z-polarized component of the electric field, increasing the thickness beyond the penetration depth of the cavity mode cannot further increase the Rabi splitting.[31] A more detailed three-dimensional representation of the E_z field distribution on resonance is presented in Figure 2b. The electric field remains localized mainly underneath the metal traces and does not expand into other regions of the semiconductor. We use this representation to calculate the mode volume on resonance for our metamaterial nanocavity, defined as the volume containing 50% of the field energy stored in the E_z component inside the semiconductor (the E_z field on the air side in this calculation is ignored).[31] This definition leads to an effective mode volume on resonance of 1.21×10^{-3} $(\lambda/n)^3$. As a comparison, we also calculated the mode volume using the standard Purcell definition and correct for dispersive media,[11,32,33] leading to a three times smaller mode volume of 3.7×10^{-4} $(\lambda/n)^3$. The more conservative, larger volume result is used in this work to obtain an upper bound for the effective mode volume.

Apart from the interaction volume, which identifies the optimum position of the QWs in our sample, we further analyze the energy conversion efficiency from incoming radiation to the E_z field in the vicinity of the metamaterial. We consider only the quantum-well stack in this calculation and ignore the E_z component in air and in the AlN cladding since
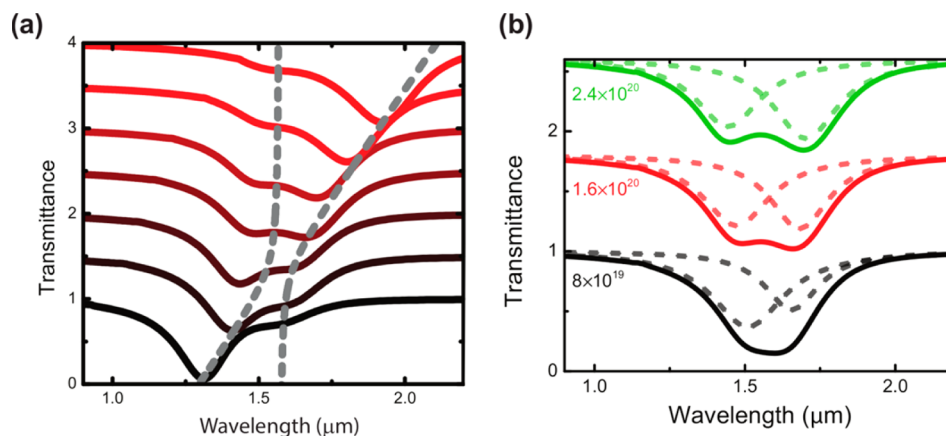
Figure 3. Calculated normal incidence transmittance curves using finite-difference time-domain simulations. (a) Calculated transmittance curves as a function of the bare cavity resonance for the medium doped sample (1.6×10^{20} cm^{-3}). The bare cavity resonance wavelength increases from the bottom line (black) to the top line (red). The dashed, gray lines are a guide to the eye representing the predicted polariton eigenfrequencies using a coupled oscillator model.[34] For clarity, the individual lines are offset vertically by 0.5. (b) Comparison of the polariton splitting for a bare cavity resonance of 1.56 μm and three different quantum-well doping levels. The dashed lines are numerical fits using two uncoupled harmonic oscillators and are meant as a guide to the eye. The individual curves are offset vertically by 0.8 for clarity.
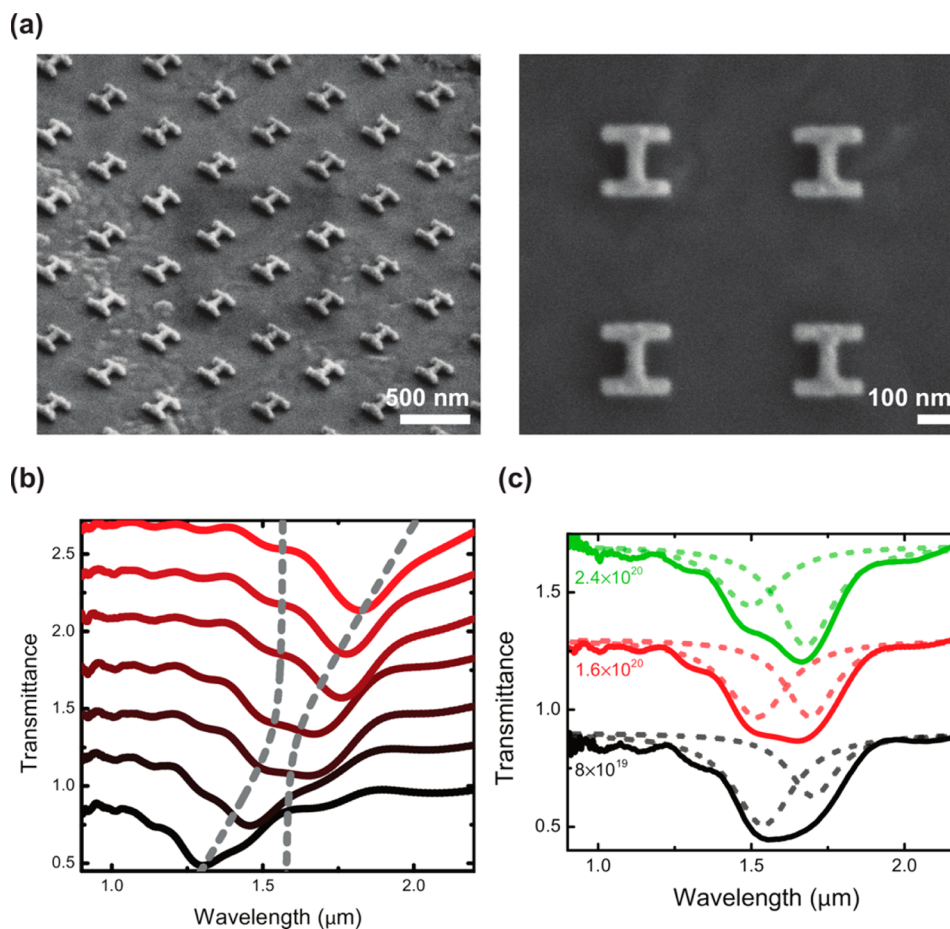

Figure 4. Fabrication and experimental transmittance results. (a) Scanning electron micrograph images showing fabricated "dogbone" nanocavities with a bare cavity resonance of 1.56 μm. The metal has a combined thickness of 55 nm (5 nm Ti adhesion layer and 50 nm Au). (b) Experimental polariton anticrossing for the medium doped sample (1.6×10^{20} cm^{-3}). The bare cavity resonance wavelength increases from the bottom line (black) to the top line (red). The dashed, gray lines are a guide to the eye showing the predicted polariton eigenfrequencies using a coupled oscillator model.[34] For clarity, the individual lines are offset vertically by 0.3. (c) Polariton splitting as a function of doping for a bare cavity resonance of 1.51 μm. The dashed lines represent a guide to the eye using two uncoupled harmonic oscillators. The polariton splitting increases with higher doping concentration, which is consistent with simulation results shown in Figure 3b. The individual curves are offset vertically by 0.4 for clarity.

these regions do not contribute to the strong coupling. The incoming plane wave is resonant with the fundamental dipolar mode of the dogbone metamaterial nanocavity ($\lambda \sim 1.56~\mu$m) and is polarized along the y-axis. We calculate the resulting field profile and integrate the electric field energy overlapping with the quantum-well for the E_z component ($W_z = \int \varepsilon_z E_z^2~dV$). The field energy W_z is referenced against the total energy of the incoming pulse to obtain the conversion efficiency. For the dogbone nanocavity this calculation shows that 39% of the incoming energy is converted to the z-polarized electric field component which overlaps with the QWs. This conversion efficiency is very high given that the dogbone nanocavities cover only 8.3% of the sample area and that the QW stack is only 238 nm thick. To analyze the strong light−matter interaction between metamaterial nanocavities and ISTs and to obtain a quantity that can be compared with experiments, we calculate the normal incidence transmittance for the coupled system. The IST resonance wavelength is kept at 1.56 μm, while the bare cavity resonance is changed by geometrically stretching the metamaterial and the unit cell. Thereby, we are able to sweep the metamaterial resonance across the IST and map out the two polariton branches which appear as minima in the transmittance spectrum. We present the simulation results for the medium doping level sample in Figure 3a, exhibiting polariton anticrossing as a function of the bare nanocavity resonance. The anticrossing appears most clearly in the case where the metamaterial and the IST have a similar uncoupled resonance frequency. The coupled system shows two minima in transmittance that are shifted toward higher (upper polariton) and lower (lower polariton) frequencies from their unperturbed values. The comparison for a constant bare cavity resonance ($\sim$1.56 μm) and the three different doping levels is shown in Figure 3b. The splitting between the two polaritons increases with higher doping concentrations as expected.[5,7,8] However, the large linewidth of the ISTs masks partly the appearance of two distinct minima in transmittance and thereby also the polariton anticrossing. We added numerical fits using two uncoupled harmonic oscillators to each simulated curve to visualize the splitting.

For the experimental verification of the strong light−matter coupling we fabricate "dogbone" metamaterial nanocavities with different bare cavity resonances atop the three differently doped samples. The metamaterial nanocavities are defined by electron beam lithography, followed by a Ti/Au (5/50 nm) evaporation and lift-off. We present scanning electron micrograph images of an array of metamaterial nanocavities with a bare metamaterial resonance of 1.56 μm in Figure 4a. Similar to the FDTD simulations, we tune the bare cavity resonance by changing the geometric size of the metamaterial nanocavities. The smallest feature sizes fabricated change from 35 nm for a bare cavity resonance wavelength of 1.2 μm to 68 nm at bare cavity resonance of 2 μm. We perform all measurements at room temperature using a Nicolet Magna 860 Fourier transform infrared spectrometer equipped with a microscope objective to control the spot size of the incident light. Thereby, we limit the measured area to $100 \times 100~\mu$m^2 to reduce the influence of wafer variation on the results. The normal incidence transmittance spectra for the medium doping level are presented in Figure 4b, showing the polariton anticrossing as a function of cavity resonance. When the uncoupled bare cavity and the IST become similar in wavelength, the transmittance exhibits two minima. This is more clearly visible by comparing the normal incidence transmittance spectra for a

bare cavity resonance of 1.51 μm and three different doping levels presented in Figure 4c. The low doped sample shows only one broadened minimum, while the medium and high doping level samples indicate two independent minima, in good agreement with simulation results.

In conclusion, we presented optical strong coupling between intersubband transitions in III-nitride heterostructures and planar "dogbone" metamaterials in the near-infrared spectral range at $\lambda \sim 1.55~\mu$m. The structures have deep subwavelength volumes of $1.21 \times 10^{-3}~(\lambda/n)^3$ and exhibit an experimental Rabi frequency of 10.1 THz, corresponding to a polariton splitting of 10% of the bare cavity frequency. The essential optical properties of the system such as dipole matrix elements, intersubband transition energies, or bare cavity frequencies can be controlled during the sample growth or fabrication. This extremely flexible system could be used to realize nonlinear optical components, electrically tunable optical filters, or intersubband LEDs. The giant nonlinearities found in ISTs combined with the strong electric field enhancement in the vicinity of metamaterial resonators can lead to highly efficient nonlinear optical processes. Tunable optical filters rely on altering the light−matter coupling between metamaterial resonators and ISTs by changing the energy of the ISTs using the quantum-confined Stark effect. The result is a continuously tunable optical filter or modulator without mechanical components. The strong coupling between metamaterial and ISTs could also be used to realize electrically pumped intersubband LEDs based on polariton emission. The major advantage of the presented metamaterial−IST system is the possibility to use the same concept and semiconductor system at any wavelength between THz and visible due to the large band offset in the conduction band offered by III-nitride heterostructures.

■ **AUTHOR INFORMATION**

Corresponding Author
*E-mail: ibrener@sandia.gov.

Notes
The authors declare no competing financial interest.

■ **REFERENCES**

(1) Khitrova, G.; Gibbs, H. M.; Kira, M.; Koch, S. W.; Scherer, A. Vacuum Rabi splitting in semiconductors. *Nat. Phys.* **2006**, *2*, 81−90.
(2) Ciuti, C.; Bastard, G.; Carusotto, I. Quantum vacuum properties of the intersubband cavity polariton field. *Phys. Rev. B* **2005**, *72*, 115303−115303.
(3) Liberato, S. D.; Ciuti, C. Quantum vacuum radiation spectra from a semiconductor microcavity. *Phys. Rev. Lett.* **2007**, *98*, 103602−103602.
(4) Dintinger, J.; Klein, S.; Bustos, F.; Barnes, W. L.; Ebbesen, T. W. Strong coupling between surface plasmon-polaritons and organic

molecules in subwavelength hole arrays. *Phys. Rev. B* **2005**, *71*, 035424−035424.

(5) Todorov, Y.; Andrews, A. M.; Colombelli, R.; Liberato, S. D.; Ciuti, C.; Klang, P.; Strasser, G.; Sirtori, C. Ultrastrong light-matter coupling regime with polariton dots. *Phys. Rev. Lett.* **2010**, *105*, 196402−196402.

(6) Scalari, G.; Maissen, C.; Turcinkova, D.; Hagenmüller, D.; Liberato, S. D.; Ciuti, C.; Reichl, C.; Schuh, D.; Wegscheider, W.; Beck, M.; Faist, J. Ultrastrong coupling of the cyclotron transition of a 2D electron gas to a THz metamaterial. *Science* **2012**, *335*, 1323−1326.

(7) Geiser, M.; Castellano, F.; Scalari, G.; Beck, M.; Nevou, L.; Faist, J. Ultrastrong coupling regime and plasmon polaritons. *Phys. Rev. Lett.* **2012**, *108*, 106402−106402.

(8) Benz, A.; Campione, S.; Liu, S.; Montano, I.; Klem, J. F.; Allerman, A.; Wendt, J. R.; Sinclair, M. B.; Capolino, F.; Brener, I. Strong coupling in the sub-wavelength limit using metamaterial nanocavities. *Nat. Commun.* **2013**, *4*, 2882−2882.

(9) Dietze, D.; Benz, A.; Strasser, G.; Unterrainer, K.; Darmo, J. Terahertz meta-atoms coupled to a quantum well intersubband transition. *Opt. Express* **2011**, *19*, 13700−13706.

(10) Delteil, A.; Vasanelli, A.; Todorov, Y.; Palma, C. F.; St-Jean, M. R.; Beaudoin, G.; Sagnes, I.; Sirtori, C. Charge-induced coherence between intersubband plasmons in a quantum structure. *Phys. Rev. Lett.* **2012**, *109*, 246808−246808.

(11) Maier, S. A. Plasmonic field enhancement and SERS in the effective mode volume picture. *Opt. Express* **2006**, *14*, 1957−1964.

(12) Lidzey, D. G.; Bradley, D. D. C.; Armitage, A.; Walker, S.; Skolnick, M. S. Photon-mediated hybridization of frenkel excitons in organic semiconductor microcavities. *Science* **2000**, *288*, 1620−1623.

(13) Schlather, A. E.; Large, N.; Urban, A. S.; Nordlander, P.; Halas, N. J. Near-field mediated plexcitonic coupling and giant Rabi splitting in individual metallic dimers. *Nano Lett.* **2013**, *13*, 3281−3286.

(14) Lee, J.; Chen, P. Y.; Argyropoulos, C.; Alu, A.; Belkin, M. A. In *Metamaterials Based on Intersubband Polaritons*; Metamaterials Congress, Bordeaux, France, 2013.

(15) Campione, S.; Benz, A.; Sinclair, M. B.; Capolino, F.; Brener, I. Second harmonic generation from metamaterials strongly coupled to intersubband transitions in quantum wells. *Appl. Phys. Lett.* **2014**, *104*, 131104−131104.

(16) Benz, A.; Montano, I.; Klem, J. F.; Brener, I. Tunable metamaterials based on voltage controlled strong coupling. *Appl. Phys. Lett.* **2013**, *103*, 263116−263116.

(17) Geiser, M.; Scalari, G.; Castellano, F.; Beck, M.; Faist, J. Room temperature terahertz polariton emitter. *Appl. Phys. Lett.* **2012**, *101*, 141118−141118.

(18) Capasso, F.; Sirtori, C.; Cho, A. Y. Coupled quantum well semiconductors with giant electric field tunable nonlinear optical properties in the infrared. *IEEE J. Quantum Elec.* **1994**, *30*, 1313−1326.

(19) Bastard, G.; Mendez, E. E.; Chang, L. L.; Esaki, L. Variational calculations on a quantum well in an electric field. *Phys. Rev. B* **1983**, *28*, 3241−3245.

(20) Miller, D. A. B.; Weiner, J. S.; Chemla, D. Electric-field dependence of linear optical properties in quantum well structures: Waveguide electroabsorption and sum rules. *IEEE J. Quantum Electron.* **1986**, *22*, 1816−1830.

(21) Faist, J.; Capasso, F.; Sirtori, C.; Sivco, D. L.; Hutchinson, A. L.; Chu, S. N. G.; Cho, A. Y. Measurement of the intersubband scattering rate in semiconductor quantum wells by excited state differential absorption spectroscopy. *Appl. Phys. Lett.* **1993**, *63*, 1354−1356.

(22) Donzelli, G.; Vallecchi, A.; Capolino, F.; Schuchinsky, A. Metamaterial made of paired planar conductors: particle resonances, phenomena and properties. *Metamaterials* **2009**, *3*, 10−16.

(23) Carlin, J.-F.; Ilegems, M. High-quality AlInN for high index contrast Bragg mirrors lattice matched to GaN. *Appl. Phys. Lett.* **2003**, *83*, 668−670.

(24) Grandusky, J. R.; Smart, J. A.; Mendrik, M. C.; Schowalter, L. J.; Chen, K. X.; Schubert, E. F. Pseudomorphic growth of thick n-type $Al_xGa_{1−x}N$ layers on low-defect-density bulk AlN substrates for UV LED applications. *J. Cryst. Growth* **2009**, *311*, 2864−2866.

(25) Wierer, J. J.; Allerman, A. A.; Li, Q. Silicon impurity-induced layer disordering of AlGaN/AlN superlattices. *Appl. Phys. Lett.* **2010**, *97*, 051907−051907.

(26) Yang, J.-S.; Sodabanlu, H.; Sugiyama, M.; Nakano, Y.; Shimogaki, Y. Blueshift of intersubband transition wavelength in AlN/GaN multiple quantum wells by low temperature metal organic vapor phase epitaxy using pulse injection method. *Appl. Phys. Lett.* **2009**, *95*, 162111−162111.

(27) Lumerical, http://www.lumerical.com.

(28) Woollam, J. A. http://www.jawoollam.com.

(29) Gabbay, A.; Brener, I. Theory and modeling of electrically tunable metamaterial devices using inter-subband transitions in semiconductor quantum wells. *Opt. Express* **2012**, *20*, 6584−6597.

(30) Campione, S.; Benz, A.; Klem, J. F.; Sinclair, M. B.; Brener, I.; Capolino, F. Electrodynamic modeling of strong coupling between a metasurface and intersubband transitions in quantum wells. *Phys. Rev. B* **2014**, *89*, 165133−165133.

(31) Benz, A.; Campione, S.; Liu, S.; Montano, I.; Klem, J. F.; Sinclair, M. B.; Capolino, F.; Brener, I. Monolithic metallic nanocavities for strong light-matter interaction to quantum-well intersubband excitations. *Opt. Express* **2013**, *21*, 32572−32581.

(32) Loudon, R. The propagation of electromagnetic energy through an absorbing dielectric. *J. Phys. A* **1970**, *3*, 233−245.

(33) Ruppin, R. Electromagnetic energy density in a dispersive and absorptive material. *Phys. Lett. A* **2002**, *299*, 309−312.

(34) Klein, M. W.; Tritschler, T.; Wegener, M.; Linden, S. Lineshape of harmonic generation by metallic nanoparticles and metallic photonic crystal slabs. *Phys. Rev. B* **2005**, *72*, 115113−115113.